Ji-Hong Li, Xu-Hui Zhu, Yan Cheng* and Guang-Fu Ji

Structural, Electronic, Elastic and Thermal Properties of Li_2AgSb: First-Principles Calculations

DOI 10.1515/zna-2015-0127
Received March 16, 2015; accepted May 4, 2015; previously published online May 28, 2015

Abstract: Based on the first-principles density functional theory calculations combined with the quasi-harmonic Debye model, the pressure dependencies of the structural, elastic, electronic and thermal properties of Li_2AgSb were systematically investigated. The calculated lattice parameters and unit cell volume of Li_2AgSb at the ground state were in good agreement with the available experimental data. The obtained elastic constants, the bulk modulus and the shear modulus revealed that Li_2AgSb is mechanically stable and behaves in a ductile manner under the applied pressure. The elasticity-relevant properties, the Young's modulus and the Poisson's ratio showed that pressure can enhance the stiffness of Li_2AgSb and that Li_2AgSb is mechanically stable up to 20 GPa. The characteristics of the band structure and the partial density of states of Li_2AgSb were analysed, showing that Li_2AgSb is a semiconductor with a direct band gap of 217 meV at 0 GPa and that the increasing pressure can make the band structure of Li_2AgSb become an indirect one. Studies have shown that, unlike temperature, pressure has little effect on the heat capacity and the thermal expansion coefficient of Li_2AgSb.

Keywords: Elastic Properties; Electronic Structures; First-Principles Calculation; Heat Capacity.

***Corresponding author: Yan Cheng,** Key Laboratory of High Energy Density Physics and Technology of Ministry of Education, Sichuan University, Chengdu 610064, China, E-mail: ycheng@scu.edu.cn; and Institute of Atomic and Molecular Physics, College of Physical Science and Technology, Sichuan University, Chengdu 610065, China
Ji-Hong Li: Institute of Atomic and Molecular Physics, College of Physical Science and Technology, Sichuan University, Chengdu 610065, China; and College of Physics and Electronic Engineering, Longdong University, Qingyang 745000, China
Xu-Hui Zhu: Institute of Atomic and Molecular Physics, College of Physical Science and Technology, Sichuan University, Chengdu 610065, China
Guang-Fu Ji: National Key Laboratory of Shock Wave and Detonation Physics, Institute of Fluid Physics, Chinese Academy of Engineering Physics, Mianyang 621900, China

1 Introduction

The topological insulator, a new state of quantum matter, has been investigated in both fundamental condensed matter physics and materials science in recent years [1–6]. Many new topological insulator materials have been theoretically predicted and experimentally observed since the topological insulator was first discovered in two-dimensional system [7, 8]. Currently known topological insulator materials can be possibly classified into two families [9]: the 2D HgTe family and the 3D Bi_2Se_3 family. Two-dimensional topological insulator materials cannot be applied in practice as they can only operate at extremely low temperature and magnetic field and at ultra-high vacuum conditions [10–12]. However, 3D topological insulator materials can be applied at room temperature and even at high temperature environment because of their simple structure and the fact that they can be easily controlled in engineering practice [1]. These give them potential application in the research fields of spintronics, fault-tolerant quantum computation, long-life catalysis, etc. [13]. Hence, researching new 3D topological insulator materials has become an important topic in the field of condensed matter physics [14–16].

In the past years, researchers mostly concentrated on chalcogenides (such as Sb_2Te_3, Bi_2Te_3 and Bi_2Se_3) for their narrow band and thermoelectric properties [17, 18]. Presently, new interest has been focused on the alkali metal-based ternary intermetallic compound X_2YZ, but only a few studies have been carried out. Lin et al. [19] predicted that the ternary intermetallic series $Li_2M'X$ (M′ = Cu, Ag, Au or Cd, and X = Sb, Bi or Sn) hosts a number of topological insulators with remarkable functional variants and tunability. They discovered that the distorted Li_2AgSb is the best lightweight ternary compound of the $Li_2M'X$ series harboring a 3D topological insulator. Li et al. [20] also predicted that the alkali metal-based ternary intermetallic compound X_2YZ (X = alkali metals, Y = Ag, Z = Sb) is a new class of 3D topological insulator. They revealed that Li_2AgSb can be realized by applying a uniaxial tensile strain of >3 % along the [001] direction.

Although Li_2AgSb has been researched as a representative of the new class of 3D topological insulators,

information about its physicochemical properties is very limited. Hence, in this work, we focused on studying the structural, elastic, electronic and thermodynamic properties of Li_2AgSb at a pressure of up to 20 GPa by employing an ab initio plane-wave pseudopotential density functional theory (DFT) method within the generalised gradient approximation (GGA) and the quasi-harmonic Debye model [21, 22]. The remaining parts of this paper are organised as follows: In Section 2, we make a brief review of the theoretical method. The obtained results are discussed carefully in Section 3. Finally, we draw the conclusions in Section 4.

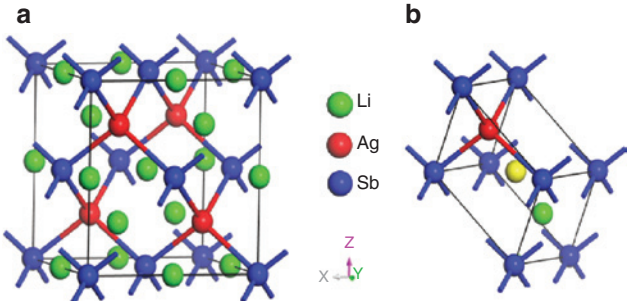

Figure 1: Crystal structure of Li_2AgSb: (a) the conventional cubic cell and (b) the primitive cell.

2 Computation Details

In this study, first-principles calculations were carried out using the CASTEP code [23]. We employed the non-local ultrasoft pseudopotentials introduced by Vanderbilt [24] for the interactions of the electrons with the ion cores in all electronic structure calculations. In order to get more accurate results, we used the 2008 revised Perdew–Burke–Ernzerhof exchange correlation functional for GGA, which can improve the equilibrium properties of densely packed solids [25]. Pseudo-atom calculations were performed for Li-$2s^2$, Ag-$4s^24p^64d^{10}5s$ and Sb-$4d^{10}\ 5s^25p^4$; the electronic wave functions were expanded by plane-wave basis set with an energy cut-off of 300 eV. The *K*-space integration was performed using $4\times4\times4$ *k*-points in the irreducible Brillouin zone. To ensure self-consistent convergence, the convergence criteria were set to 1.0×10^{-5} eV/atom for the total energy, 0.03 eV/Å for the maximum force, 0.05 GPa for the maximum stress and 0.001 Å for the maximum displacement. In the calculation of elastic properties, the criteria of convergence were set to 2×10^{-6} eV/atom for the energy, 0.006 eV/Å for the maximum force, 2×10^{-4} for the maximum displacement and 0.003 GPa for the maximum strain amplitude. Phonon calculations were performed by using the finite displacement method using the same pseudopotentials as implemented in the CASTEP code. These parameters were carefully tested and were proven to be good enough to lead to well-converged total energy and lattice parameters.

3 Results and Discussion

3.1 Structure and Equation of States

Figure 1 shows the conventional cell and primitive cell of Li_2AgSb. At ambient conditions, the crystal lattice of Li_2AgSb belongs to the space group F-43m (no. 216); the atomic arrangements are as follows: The Ag and Sb atoms occupy the Wyckoff 4d (0.75, 0.75, 0.75) and 4a (0, 0, 0) positions, respectively. The Li atoms fill the remaining empty space in the 4b (0.5, 0.5, 0.5) and 4c (0.25, 0.25, 0.25) positions. In order to obtain the ground state structure of Li_2AgSb, we used different primitive cell volume V of Li_2AgSb and then calculated the corresponding energy E. We obtained a series of $E - V$ (Fig. 2) data from Li_2AgSb [the unit of energy E and volume V are shown in units of Hartree and $Bohr^3$, respectively, to fit the equation of state (EOS)]. By fitting the $E - V$ data to the third-order Birch–Murnaghan EOS [26], we obtained the equilibrium structural parameters a and cell volume V_0, as well as the bulk modulus B_0 and its pressure derivative B_0' of Li_2AgSb at 0 K and 0 GPa. Our calculated results, together with the available experimental data [27], are listed in Table 1. For structural parameter a, our result was well consistent with the experimental data, with an error of about 0.15 %.

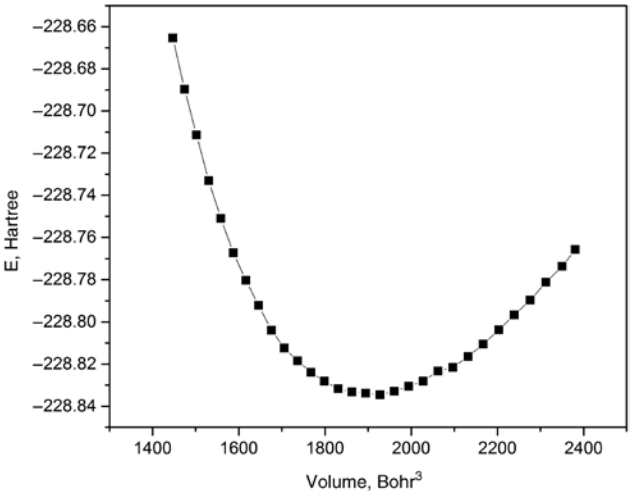

Figure 2: Energy as a function of unit cell volume of Li_2AgSb.

Table 1: Calculated equilibrium lattice parameter a, cell volume V_0, bulk modulus B_0 and its pressure derivative B_0' of Li_2AgSb at 0 K and 0 GPa, together with the available experimental data.

Method	a (Å)	V_0 (Å^3)	B_0 (GPa)	B_0'
Calculated (GGA-PBESOL)	6.593	286.563	52.72	4.80
Experimental[a] [27]	6.583	285.280		

[a]Obtained from the X-ray diffraction measurements.

GGA-PBESOL, Perdew–Burke–Ernzerhof exchange correlation functional for generalized gradient approximation.

The obtained bulk modulus B_0 was about 51.82 GPa and its pressure derivative B_0' was 4.80. The bulk modulus calculated by this method was in good agreement with that deduced from the elastic constants (52.19 GPa in Table 2). Unfortunately, at present, there are no other theoretical or experimental data that can be used for comparison.

3.2 Elastic and Mechanical Properties

The elastic properties of the materials are closely related to various fundamental solid-state properties such as the Debye temperature, thermal expansion, mechanical stability of the materials, etc. Hence it is meaningful to study the elastic properties of Li_2AgSb. The elastic constants C_{ijkl} ($i, j, k, l = 1$–6) of the materials can be formulated as $C_{ijk} = \left(\frac{\partial \sigma_{ij}(x)}{\partial e_{kl}}\right) X$ [28, 29], where σ_{ij} is the applied stresses, e_{kl} is the strains, and X and x are the coordinates before and after deformation, respectively. We can use a series of small strains on the crystal lattice and then get the corresponding stresses expressed by certain elastic constants, and the individual elastic constant can be obtained by solving these equations.

For cubic Li_2AgSb, there are three independent elastic constants, i.e., C_{11}, C_{12}, C_{44}. In Table 2, we list the calculated elastic constants C_{ij} of Li_2AgSb at a pressure range from 0 to 20 GPa. Figure 3 shows the pressure dependence of the elastic constants. We can see that the elastic constants C_{11} and C_{44} increased rapidly with increasing pressure, whereas the elastic constant C_{12} increased comparatively slowly. It can also be seen that the elastic constants satisfied the following stability conditions [30]: $C_{44}' > 0$, $C_{11}' > |C_{12}'|$, $C_{11}' + 2C_{12}' > 0$, where $C_{\alpha\alpha}' = C_{\alpha\alpha} - P$ ($\alpha = 1, 4$), $C_{12}' = C_{12} + P$, indicating that Li_2AgSb is mechanically stable in the pressure range from 0 to 20 GPa. To make sure Li_2AgSb was stable up to 20 GPa, we present the calculated phonon dispersion curves of Li_2AgSb at pressure levels of 0, 10 and 20 GPa in Figure 4a–c, respectively. It can be seen that the frequencies of all phonon branches in the whole Brillouin zone have positive values, i.e., the Li_2AgSb crystal can remain stable up to 20 GPa.

According to the Voigt–Reuss–Hill approximations [31] and from the calculated elastic constants C_{ij}, the Voigt shear modulus G_V, Reuss shear modulus G_R, bulk modulus B and shear modulus G can be, respectively, obtained as follows: $G_V = (C_{11} - C_{12} + 3C_{44})/5$, $G_R = 5(C_{11} - C_{12})\, C_{44}/[4C_{44} +$

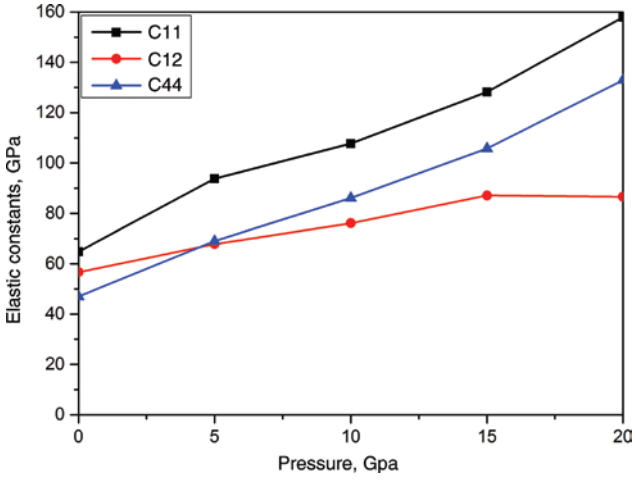

Figure 3: Calculated elastic constants of Li_2AgSb as a function of pressure.

Table 2: Calculated elastic constants C_{ij} (GPa), bulk modulus B (GPa), shear modulus G (GPa), B/G values, Young's modulus E (GPa) and Poisson's ratio σ of Li_2AgSb at different hydrostatic pressure levels.

p	C_{11}	C_{12}	C_{44}	B	G	B/G	E	σ
0	63.634	46.462	56.125	52.186	27.284	1.913	24.419	0.422
5	95.222	70.630	67.657	78.827	34.834	2.263	35.065	0.426
10	107.846	86.956	76.908	93.919	36.008	2.608	30.214	0.446
15	129.230	106.331	87.036	113.964	40.354	2.824	33.235	0.451
20	154.718	131.732	88.658	139.393	40.922	3.406	33.553	0.460

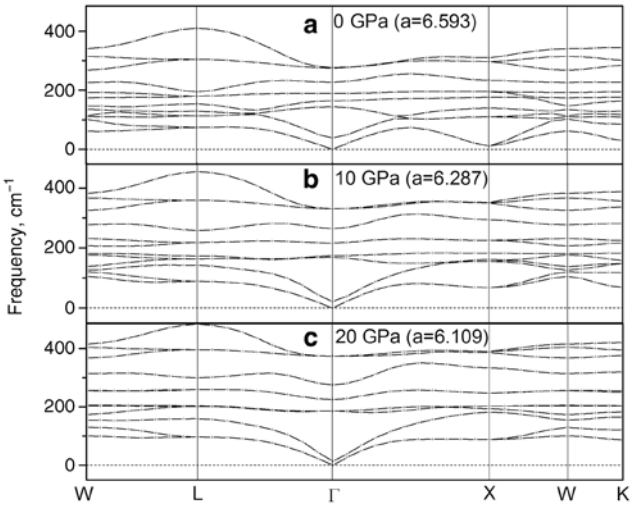

Figure 4: Calculated phonon dispersion curves of Li_2AgSb at 0 GPa (a), 10 GPa (b) and 20 GPa (c).

$3(C_{11} - C_{12})]$, $B = (C_{11} + 2C_{12})/3$, $G = (G_V + G_R)/2$. The values of B and G of Li_2AgSb at different pressure levels are shown in Table 2, together with the value of B/G. Figure 5 shows that the bulk modulus B increased rapidly with increasing pressure, whereas the shear modulus G increased slowly under pressure. Pugh [32] suggested that the value of B/G is associated with the ductility or brittleness of a material. The critical value is 1.75. If $B/G < 1.75$, the material behaves in a brittle manner; otherwise, the material behaves in a ductile manner. Our calculated result shows that the value of B/G was larger than 1.75 at a pressure range from 0 GPa to 20 GPa, indicating that Li_2AgSb is ductile in this pressure range. We can see that the value of B/G increased with increasing pressure, indicating that pressure can enhance the ductility of Li_2AgSb.

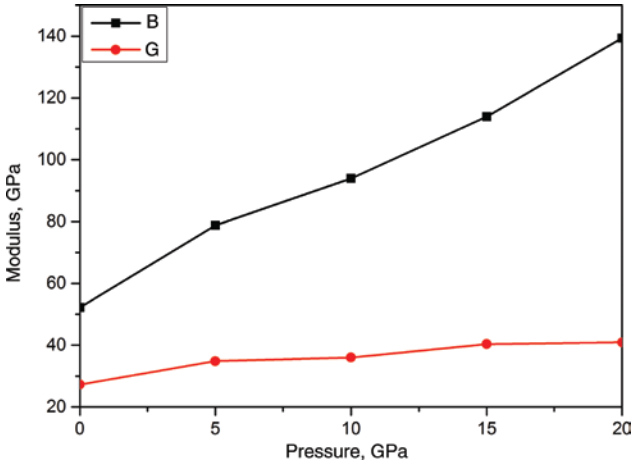

Figure 5: Calculated bulk modulus (B) and shear modulus (G) of Li_2AgSb as a function of pressure.

Young's modulus (E) and Poisson's ratio (σ) can be calculated from the bulk modulus (B) and shear modulus (G), respectively, as follows: $E = 9BG/(3B + G)$, $\sigma = (3B - E)/6B$. Young's modulus (E) reflects the stiffness of a crystal. The larger the value of E, the stiffer the crystal. In our calculations, the E value of Li_2AgSb was 24.42 GPa at 0 GPa and it increased slowly with increasing pressure, indicating that the pressure enhances the stiffness of Li_2AgSb. Poisson's ratio reflects the stability of a crystal against shear. It is the ratio of transverse contraction strain vs. longitudinal extension strain under a stretching force. The variation of the Poisson's ratio of Li_2AgSb was very small, from 0 to 20 GPa, indicating again that Li_2AgSb is stable when sheared. In contrast, Poisson's ratio provides information about the characteristics of the bonding forces. For central force solids, the lower limit of Poisson's ratio is 0.25 and the upper limit is 0.5 [33]. The Poisson's ratio of Li_2AgSb is larger than 0.25 but <0.5, suggesting that the interatomic forces in Li_2AgSb are central at a pressure range from 0 to 20 GPa.

3.3 Electronic Structures

The density of states (DOS) plays an important role in the analysis of the physical properties of materials. In this work, we performed an analysis on the changes in the DOS of Li_2AgSb at several pressure levels. We illustrate here the calculation of the partial density of states (PDOS) and total density of states (TDOS) at 0 and 20 GPa. At 0 GPa (Fig. 6a), the lower valence band (located at –11 to –9 eV) is composed of the Sb-5s, Ag-4p and Ag-4d states, and it is dominated by the Sb-5s state. The middle valence band (located at –7 to –4 eV) is dominated by the Ag-4d state with little contribution from the Sb-5p and Li-2s states. The upper valence band (located at –4 to 0 eV) is mainly composed of the Sb-5p and Li-2s states. We can see from Figure 6a that the valence bands are mainly dominated by the Ag-4d state located at 5.65 eV. In the conduction band, the Sb-5s, Ag-4p and Li-2s states play the dominant role from 0 to 5 eV; the region from 5 to 8 eV consists of the Sb-5s, Sb-5p and Li-2s states, and the range from 8 to 14 eV primarily consists of the Ag-4p and Li-2s states. From the aforementioned analysis, in the whole valence band, it can be seen that the Ag-4p, Ag-4d and Sb-5s states hybridize in the energy range from –11 to –9 eV and that the Sb-5p state strongly hybridizes with the Li-2s state from –7 to 0 eV. These hybridizations imply the existence of covalent bonding in Li_2AgSb. In Figure 6b, we can see that the DOS

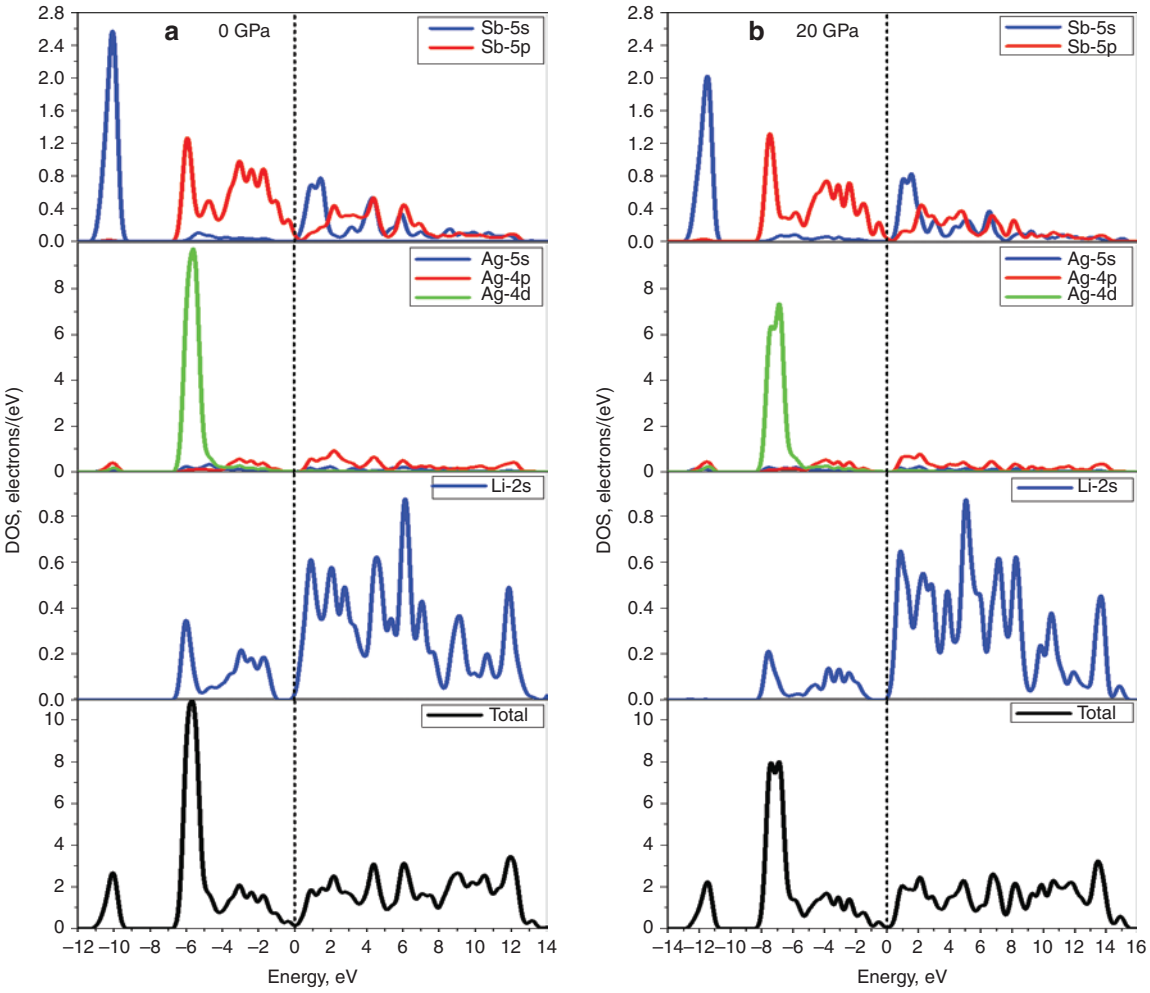

Figure 6: Calculated total density of states and partial density of states of Li_2AgSb at 0 GPa (a) and 20 GPa (b).

of Li_2AgSb at 20 GPa somewhat differs from that at 0 GPa. Firstly, at 20 GPa, the peaks of TDOS and PDOS become smaller in the energy range studied. Secondly, at 20 GPa, the range of the upper valence bands becomes wider. The middle valence band and the lower valence band move slightly to the lower energy end.

Moreover, we also calculated the band structure of Li_2AgSb along the high-symmetry directions at 0 GPa (Fig. 7a), 5 GPa (Fig. 7b), 10 GPa (Fig. 7c), 15 GPa (Fig. 7d) and 20 GPa (Fig. 7e). It is clear from Figure 7a that Li_2AgSb at 0 GPa is a semiconductor with a direct band gap of 217 meV. The valence band maximum and the conduction band minimum are all at the Γ point. In Figure 7b–e, we can see that the band gap gradually broadened with increasing pressure and the conduction band minimum gradually moved to the X point. When the pressure increased to 20 GPa, it became an indirect crystal with a band gap of 360 meV.

3.4 Thermal Properties

To explore the thermodynamic properties of Li_2AgSb, we used an approximation method based on a quasi-harmonic Debye model [21, 22] and combined it with the first-principle calculation of *E-V* relationship (Fig. 2) to solve the nonequilibrium Gibbs function $G^*(V, p, T) = E(V) + PV + A_{vib}(\Theta(V), T)$, where $E(V)$ is the total energy as a function of the cell volume V, P is the hydrostatic pressure, $\Theta(V)$ is the Debye temperature as a function of V and A_{vib} is the vibrational Helmholtz free energy (see [21] for details). Based on this model, the specific heats C_V and C_P and the thermal expansion coefficient α can be deduced from the following expressions: $Cv = 3nk\left[4D\left(\frac{\Theta}{T}\right) - \left(\frac{3\Theta/T}{e^{\Theta/T}-1}\right)\right]$, $C_P = C_V(1 + \gamma\alpha T)$, $\alpha = \gamma C_V/B_T V$, where B_T is the static bulk modulus and γ is the Grüneisen parameter, which can be

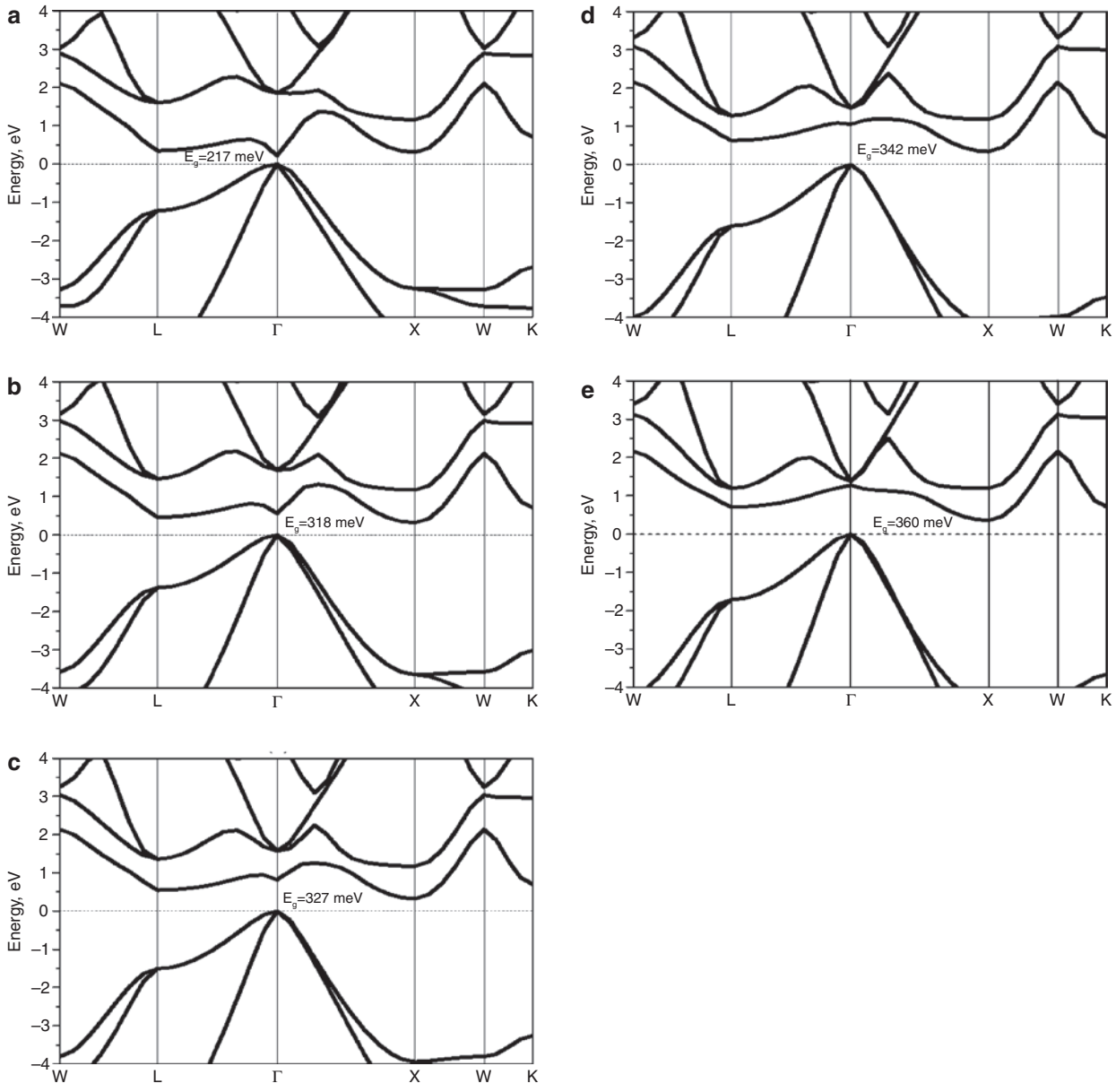

Figure 7: Band structure of Li_2AgSb at 0 GPa (a), 5 GPa (b), 10 GPa (c), 15 GPa (d) and 20 GPa (e).

derived from $B_T(P, T) = V[\partial^2 G^*(V, P, T)/\partial V^2]_{P,T}$ and $\gamma = -d \ln \Theta(V)/d \ln V$, respectively.

Figure 8 shows the calculated results of the specific heats C_V and C_P of Li_2AgSb as a function of temperature T at 0 GPa. It indicates that the heat capacity C_P (heat capacity at constant pressure) and C_V (heat capacity at constant volume) increased rapidly at a temperature below 400 K, whereas above it, C_P increased gradually; in contrast, C_V increased gently. At 500 K, C_V was 97.24 J/(mol K), approaching the Dulong–Petit limit $3nN_AK_B$ [99.72 J/(mol K)]. Figure 9 shows that the C_V and C_P of Li_2AgSb varied with the temperature at a pressure range from 0 to 20 GPa. It shows that, at any given pressure, C_P and C_V rose steeply with increasing temperature at the beginning and then the capacity of C_P increased slowly, whereas the capacity of C_V increased mildly. At any given temperature, C_P and C_V decreased when the pressure became higher. With the increase in temperature, the differences in capacity at different pressure levels became more and more inconspicuous for C_V. We can see that pressure had little effect on C_V and C_P compared to the temperature. Increasing the pressure resulted only in a small decrease in heat capacity. This decrease can be attributed to the contribution of the reduced atomic vibration amplitude caused by the increased pressure [34].

Figure 10 shows the thermal expansion coefficient of Li_2AgSb as a function of both temperature and pressure.

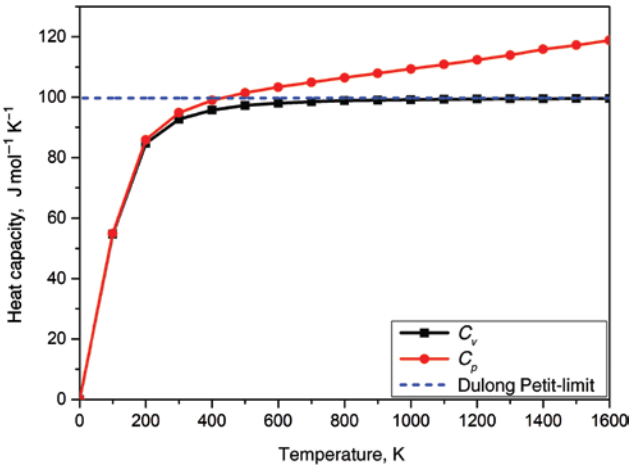

Figure 8: Heat capacity C_p and C_V of Li_2AgSb as a function of temperature T at 0 GPa.

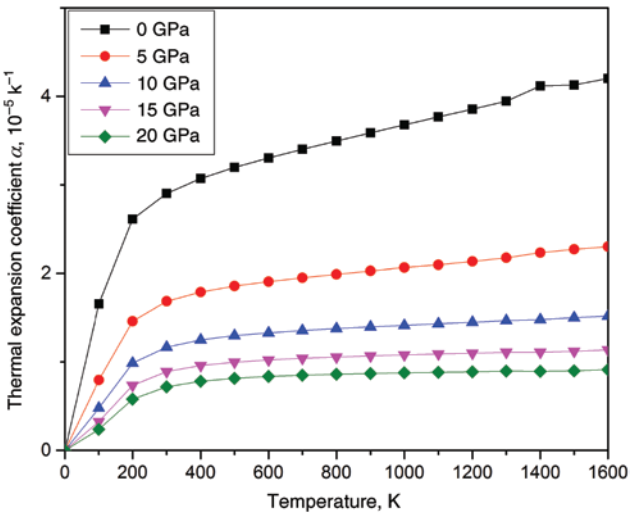

Figure 10: Thermal expansion coefficient α of Li_2AgSb as a function of temperature T at selected pressure levels.

We can see that, with increasing temperature, the thermal expansion coefficient increased rapidly from the start and gradually achieved a constant value. At a given temperature, the thermal expansion coefficient decreased when the pressure increased, and the higher the pressure, the smaller the decrease in thermal expansion coefficient.

4 Conclusions

We investigated the structure, electronic, mechanical and thermal properties of Li_2AgSb under pressure by utilizing the first-principles method based on the DFT and quasi-harmonic Debye mode. The calculated elastic constants indicated that the elastic properties of Li_2AgSb are strongly pressure dependent. The elastic constants C_{11}, C_{12} and C_{44} increased with increasing pressure. The analyses on the band structure and the partial density of states revealed that the valence bands of Li_2AgSb were mainly dominated by the Ag-4p state located at 5.5 eV. In the conduction band, the Ag-4p and Li-2s states played the dominant role from 0 to 14 eV. In addition, at ground state, the band structure of Li_2AgSb was a semiconductor with a direct band gap of 217 meV. With increasing pressure from 0 to 20 GPa, Li_2AgSb became an indirect crystal with a band gap of 360 meV. Thermal calculations showed that the specific heats C_V and C_p and the thermal expansion coefficient increased rapidly at a temperature below 400 K, whereas above it, the trend was slower.

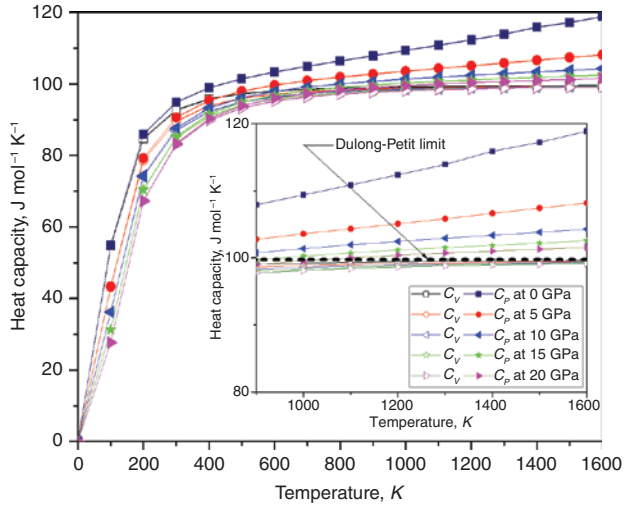

Figure 9: Heat capacity C_p and C_V of Li_2AgSb as a function of temperature T at selected pressure levels.

References

[1] Y. L. Chen, J. G. Analytis, J. H. Chu, Z. K. Liu, S. K. Mo, X. L. Qi, Z. X. Shen, Science **325**, 178 (2009).
[2] X. L. Qi, S. C. Zhang, Phys. Today **63,** 33 (2010).
[3] M. Z. Hasan, C. L. Kane, Rev. Mod. Phys. **82,** 3045 (2010).
[4] X. L. Qi, S. C. Zhang, Rev. Mod. Phys. **83,** 1057 (2011).
[5] L. Müchler, H. Zhang, S. Chadov, B. Yan, F. Casper, J. Kübler, S. C. Zhang, C. Felser, Angew. Chem. Int. Ed. **51,** 7221 (2012).
[6] C. Z. Chang, J. Zhang, X. Feng, J. Shen, Z. Zhang, M. Guo, Q. K. Xue, Science **340,** 167 (2013).
[7] B. A. Bernevig, T. L. Hughes, and S. C. Zhang, Science **314,** 1757 (2006).
[8] M. König, S. Wiedmann, C. Brüne, A. Roth, H. Buhmann, L. Molenkamp, X. L. Qi, S. C. Zhang, Science **318,** 766 (2007).

[9] B. Yan, S. Zhang, Rep. Prog. Phys. **75,** 96501 (2012).
[10] Y. G. Yao, F. Ye, X. L. Qi, S. C. Zhang, Z. Fang, Phys. Rev. B **75,** 041401 (R) (2007).
[11] D. Huertas-Hernando, F. Guinea, A. Brataas, Phys. Rev. B **74,** 155426 (2006).
[12] H. Min, J. E. Hill, N. A. Sinitsyn, B. R. Sahu, L. Kleinman, A. H. MacDonald, Phys. Rev. B **74,** 165310 (2006).
[13] L. Fu, C. L. Kane, E. J. Mele, Phys. Rev. Lett. **98,** 106803 (2007).
[14] G.J. Snyder, E.S. Tobere, Nat. Mater. **7,** 105 (2008).
[15] Y. Q. Cao, X. B. Zhao, T. J. Zhu, X. B. Zhang, J. P. Tu, Appl. Phys. Lett. **92,** 143106 (2008).
[16] K. Kadel, L. Kumari, W. Z. Li, J. Y. Huang, P. P. Provencio, Nanoscale Res. Lett. **6,** 57 (2011).
[17] H. Zhang, C.X. Liu, X.L. Qi, X. Dai, Z. Fang, S.C. Zhang, Nat. Phys. **5,** 438 (2009).
[18] W. Zhang, R. Yu, H.J. Zhang, X. Dai, Z. Fang, New J. Phys. **12,** 065013 (2010).
[19] H. Lin, T. Das, Y. J. Wang, L. A. Wray, S.-Y. Xu, M. Z. Hasan, A. Bansil, Phys. Rev. B **87,** 121202 (R) (2013).
[20] N. Li, K. L. Yao, X. J. Zhao, Comput. Mater. Sci. **91,** 231 (2014).
[21] M.A. Blanco, E. Francisco, V. Luaña, Comput. Phys. Commun. **158,** 57 (2004).
[22] Y. Zhang, X. Ke, C. Chen, J. Yang, P. Kent, Phys. Rev. B **80,** 024304 (2009).
[23] M. D. Segall, P. J. D. Lindan, M. J. Probert, C. J. Pickard, P. J. Harsnip, S. J. Clark, M. C. Panye, J. Phys.: Condens. Matter **14,** 2717 (2002).
[24] D. Vanderbilt, Phys. Rev. B **41,** 7892 (1990).
[25] J. P. Perdew, A. Ruzsinszky, G. I. Csonka, O. A. Vydrov, G. E. Scuseria, L. A. Constantin, K. Burke, Phys. Rev. Lett. **100,** 136406 (2008).
[26] S. Baroni, S. de Gironcoli, A. Dal Corso, P. Giannozzi, Rev. Mod. Phys. **73,** 515 (2001).
[27] H. Pauly, A. Weiss, H. Witte, Z. Metallkunde **59,** 47 (1968).
[28] D.C. Wallace, Thermodynamics of Crystals, Wiley, New York 1972.
[29] J. Wang, S. Yip, S. R. Phillpot, D. Wolf, Phys. Rev. B **52,** 12627 (1995).
[30] G. V. Sin'ko, N. A. Smirnov, Phys.: Condens. Matter, **14,** 6989 (2002).
[31] R. Hill, Proc. Soc. Lond. A **65,** 349 (1952).
[32] S. F. Pugh, Philos. Mag. **45,** 823 (1954).
[33] F. Chu, Y. He, D. J. Thoma, T. E. Mitchell, Scripta Metall. Mater. **33,** 1295 (1995).
[34] J. Sólyom, P. Attila, Fundamentals of the Physics of Solids: Structure and Dynamics, Vol. 2, Springer-Verlag, Berlin, 2009.